JOURNAL OF GUIDANCE, CONTROL, AND DYNAMICS
Vol. 34, No. 4, July–August 2011

Optimal Formation Design for Magnetospheric Multiscale Mission Using Differential Orbital Elements

Christopher W. T. Roscoe,* Srinivas R. Vadali,† Kyle T. Alfriend,‡ and Uri P. Desai§
Texas A&M University, College Station, Texas 77843-3141

DOI: 10.2514/1.52484

The Magnetospheric Multiscale Mission requires a formation of four satellites in a nearly regular tetrahedron throughout a region of interest defined near the apogee of a highly eccentric reference orbit. Previous papers have addressed the design of formations in orbits of high eccentricity to maximize a quality factor in a region of interest, including the use of differential mean orbital elements as design variables. In this paper, a robust optimization method is presented to improve formation performance in the presence of formation initialization errors. Several design methods are analyzed by applying differential semimajor axis errors, which have a strong effect on the long-term stability of spacecraft formations. It is shown that large formations can satisfy mission requirements for a longer time than smaller formations, when the same magnitude of errors are considered, and generally exhibit less variation in quality factors due to these errors. The robust optimization method is applied to these smaller formations and produces results that are much more stable when semimajor axis errors are included, at a cost of some performance in the nominal error-free case. The results are verified using the NASA General Mission Analysis Tool and are shown to be reasonably accurate, except in predicting very long-term behavior. A physical analysis of the geometry of several magnetospheric multiscale formation designs is provided, and eight distinct optimal tetrahedron orientations are identified (two configurations, in which the chief satellite can be placed at any of the four vertices).

I. Introduction

THE objective of the Magnetospheric Multiscale (MMS) Mission is to study magnetic reconnection, charged particle acceleration, and turbulence in key boundary regions of the Earth's magnetosphere [1]. The mission will employ a unique orbital strategy of two main phases, in which the reference orbit apogee is placed at 12 R_e and 25 R_e, respectively. With the perigee of both phases at 1.2 R_e, this means a highly eccentric orbit, with $e = 0.81818$ in Phase I and $e = 0.9084$ in Phase II. This high eccentricity, combined with a moderate inclination of 28.5° (which makes the J_2 perturbation a significant factor), and the long duration of the mission make the design of a high-quality stable formation a challenging prospect. Furthermore, the satellites can only be maneuvered during certain portions of the orbit, when science data are not being collected, and each one is spinning, which makes it difficult to accurately execute a given maneuver. Thus, once such a formation has been designed, the limitations of onboard systems make it impossible to initialize the desired formation exactly.

Both phases of the MMS mission call for a formation of four satellites, which are to form a nearly regular tetrahedron near apogee. Phase I requires tetrahedra with side lengths of 10, 25, 60, and 160 km; Phase II requires side lengths of 30, 60, 160, and 400 km. The quality factor is a metric used to compare the size and shape of the instantaneous tetrahedron with a regular tetrahedron of acceptable size, defined on a range from 0 to 1, with 1 indicating a regular tetrahedron of acceptable size. The mission requires a quality factor which exceeds 0.7 for 80% of the time spent in the science region of interest (ROI), defined as all portions of the orbit above a radius of 9 R_e for Phase I and 15 R_e for Phase II. Additionally, for collision avoidance, the spacecraft must remain at least 4 km apart at all times, and separations of greater than 6 km are desired near perigee due to the high speeds at which the spacecraft travel in that region. This paper will focus on Phase I of the MMS mission, for which the definition of the ROI results in a true anomaly range of approximately ±20° of apogee.

A general method for designing formations to satisfy science return criteria was presented by Hughes [2] and applied to the single-orbit design of an MMS formation. The long-term formation design problem was addressed by Hughes [3] using a multirevolution optimization approach with Cartesian position and velocity as the design parameters. Gim and Alfriend [4] presented a formation design approach for the MMS mission using differential mean orbital elements, and they investigated a number of properties of the tetrahedron formations, such as their initial orientation with respect to the orbital frame. Differential orbital elements are a natural and convenient choice for designing general formations [5], and using mean elements allows for the explicit inclusion of secular effects due to J_2. Griffith et al. [6,7] presented another method of designing satellite formations (including tetrahedral formations) for tracking missions using differential elements, which penalizes expected maintenance maneuver fuel expenditure in order to reduce relative drift due to J_2. The formation initialization process using differential mean orbital elements was generalized by Roscoe et al. [8] for an arbitrarily oriented regular tetrahedron, and two fast optimization approaches were presented using the Gim–Alfriend (G–A) state transition matrix (STM) [9].

Several analytical theories exist to describe the relative motion of satellites in elliptic reference orbits in closed form [9–14], and a comparison of the accuracy of various theories was performed by Alfriend and Yan [15]. Gim and Alfriend [9] derived a solution based on the relationship between the relative state and the differential orbital elements, which includes both the reference orbit eccentricity and the first-order absolute and differential J_2 perturbation effects. Using this method to propagate the tetrahedron configuration, along with the choice of differential mean orbital elements as the design

Presented as Paper 2010-7958 at the AIAA/AAS Astrodynamics Specialist Conference, Toronto, Ontario, Canada, 2–5 August 2010; received 20 September 2010; revision received 4 March 2011; accepted for publication 6 March 2011.

*Graduate Student, Department of Aerospace Engineering, Mail Stop 3141; c.roscoe@tamu.edu. Student Member AIAA.

†Stewart and Stevenson Professor, Department of Aerospace Engineering, Mail Stop 3141; svadali@tamu.edu. Associate Fellow AIAA.

‡Texas Engineering Experiment Station Distinguished Research Chair Professor, Department of Aerospace Engineering, Mail Stop 3141; alfriend@tamu.edu. Fellow AIAA.

§Undergraduate Research Assistant, Department of Aerospace Engineering, Mail Stop 3141; u_desai@tamu.edu.

parameters, provides a very efficient optimization scheme for the formation design problem.

In this paper, the long-term stability of MMS Phase I formations is investigated in the presence of expected maneuver and navigation errors estimated by Hughes [3]. After analyzing the performance of the formation design methods presented by Roscoe et al. [8], a robust optimization approach is introduced to reduce the error sensitivity of the formation lifetime, which uses the modified along-track drift condition of [8]. Finally, the simulation results are verified using the NASA General Mission Analysis Tool (GMAT), and a physical interpretation of the various formation design methods is offered. These results provide a method for mission designers to explicitly include the effects of errors in the optimal design process, which has important practical implications for MMS and beyond.

II. Problem Definition

The initial design of a tetrahedron formation using differential mean orbital elements is described in detail by Roscoe et al. [8]. A tetrahedron formation and associated reference frame $\mathcal{T}$ are shown in Fig. 1. One satellite, 0, is placed at the origin of this frame, and it is designated the chief or reference satellite (to follow the reference orbit). The other three satellites (1, 2, and 3) are placed at the remaining vertices of the tetrahedron, and they are designated the deputies. The position of the jth satellite relative to the chief is defined as $\mathbf{r}_j$, and its orbit position is $\mathbf{R}_j$. Frame $\mathcal{T}$ is defined with $\hat{\mathbf{t}}_1$ in the direction of 1; with $\hat{\mathbf{t}}_2$ in the plane of 1 and 2, oriented such that $\mathbf{r}_2 \cdot \hat{\mathbf{t}}_2 > 0$; and with $\hat{\mathbf{t}}_3$ completing the right-hand coordinate system. Note that the ordering of the deputies can always be chosen such that $\mathbf{r}_3 \cdot \hat{\mathbf{t}}_3 > 0$ as well.

Frame $\mathcal{T}$ is related to the local-vertical–local-horizontal (LVLH) frame, $\mathcal{H}$ (shown in Fig. 2), of the reference satellite by a 3-2-1 (ϕ-ψ-γ) Euler rotation sequence

$$\mathbf{C}_{\text{th}} = \mathbf{C}_1(\gamma)\mathbf{C}_2(\psi)\mathbf{C}_3(\phi) \tag{1}$$

which allows for the definition of a tetrahedron of any possible orientation in the LVLH frame. To minimize linearization errors in the transformation between relative position and velocity and differential orbital elements, the LVLH curvilinear coordinate system (frame $\mathcal{C}$) is used. This system is illustrated in Fig. 3 and has the same orientation as the LVLH frame, but the first coordinate x is the difference in the orbit radii, and the second and third coordinates, y and z, are the curvilinear distances along imaginary circular orbits in the reference orbital plane and perpendicular to the reference orbit, respectively. Expressing the relative position and velocity in curvilinear coordinates, the state of the jth satellite is defined as

$$\mathbf{x}_j = \begin{bmatrix} {}^{c}\mathbf{r}_j \\ {}^{c}\dot{\mathbf{r}}_j \end{bmatrix} \tag{2}$$

The nonsingular mean orbital elements of the reference orbit are defined as

$$\mathbf{e} = [\,a \quad \theta \quad i \quad q_1 \quad q_2 \quad \Omega\,]^T \tag{3}$$

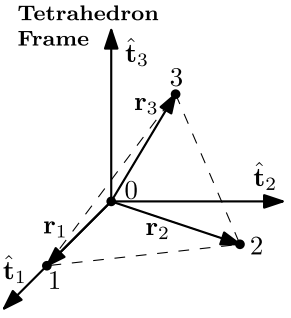

Fig. 1 Geometry of a regular tetrahedron.

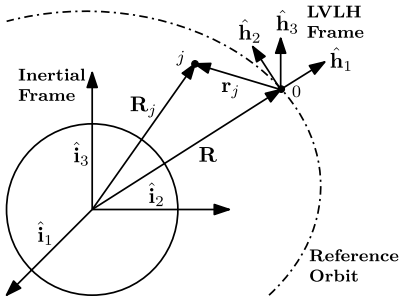

Fig. 2 LVLH reference frame.

where a is the semimajor axis, $\theta = f + \omega$ is the true argument of latitude, f is the true anomaly, ω is the argument of perigee, $q_1 = e\cos\omega$ and $q_2 = e\sin\omega$ are the orbital frame components of the eccentricity vector, e is the eccentricity, and Ω is the right ascension of the ascending node. This set of orbital elements is chosen instead of the classical orbital elements, because it is not singular in the case of a circular orbit; however, it will still be singular in an equatorial orbit.

The initial differential mean orbital elements of the jth satellite are

$$\begin{aligned}\delta\mathbf{e}_j &= [\,\delta a_j \quad \delta\theta_j \quad \delta i_j \quad \delta q_{1j} \quad \delta q_{2j} \quad \delta\Omega_j\,]^T \\ &= [\mathbf{D}(t_0)]^{-1}[\boldsymbol{\Sigma}(t_0)]^{-1}\mathbf{x}_j(t_0)\end{aligned} \tag{4}$$

where

$$\mathbf{D}(t) = \frac{\delta\mathbf{e}_{\text{osc}}}{\delta\mathbf{e}_{\text{mean}}} \tag{5}$$

is the transformation matrix between the relative mean and osculating elements, and $\boldsymbol{\Sigma}(t)$ is the transformation matrix between the relative osculating elements and the curvilinear state. Similarly, the curvilinear state $\mathbf{x}_j$ of the jth satellite can be computed at an arbitrary time t from its initial differential mean orbital elements $\delta\mathbf{e}_j$ using the G–A STM

$$\mathbf{x}_j(t) = \boldsymbol{\Sigma}(t)\mathbf{D}(t)\boldsymbol{\phi}_{\mathbf{e}}(t, t_0)\delta\mathbf{e}_j \tag{6}$$

where $\boldsymbol{\phi}_{\mathbf{e}}(t, t_0)$ is the STM for the relative mean elements. Note that, although the argument (t_0) is omitted from $\delta\mathbf{e}_j$, these represent the initial differential mean orbital elements. The matrices $\boldsymbol{\Sigma}(t)$, $\mathbf{D}(t)$, and $\boldsymbol{\phi}_{\mathbf{e}}(t, t_0)$ can be found in [9].

A. Along-Track Drift Condition

To obtain bounded relative motion in the presence of J_2, a constraint must be applied to the in-plane angular rate of each satellite with respect to the reference orbit. For small $\delta\Omega_j$ and δi_j, the condition to minimize the average along-track drift throughout an orbit is [16]

$$\delta\dot{M}_j + \delta\dot{\omega}_j + \delta\dot{\Omega}_j\cos i = 0 \tag{7}$$

To the first order in J_2, the change in the semimajor axis required to enforce this constraint is

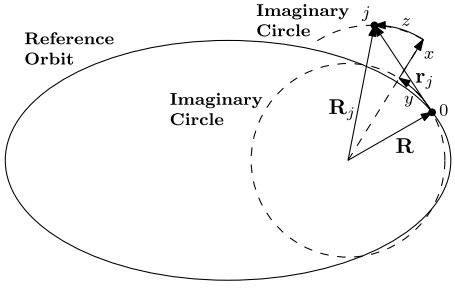

Fig. 3 LVLH curvilinear reference frame.

$$\delta a_j = \frac{J_2 R_e^2 (3\eta + 4)}{2a\eta^4}\left[(3\cos^2 i - 1)\frac{e\delta e_j}{\eta^2} - \sin 2i\ \delta i_j\right] \tag{8}$$

where $\eta = \sqrt{1-e^2}$. This result is obtained by taking the first variation of the mean rates

$$\dot{M} = n + \frac{3}{4}J_2 n\left(\frac{R_e}{p}\right)^2 \eta(3\cos^2 i - 1) \tag{9}$$

$$\dot{\omega} = \frac{3}{4}J_2 n\left(\frac{R_e}{p}\right)^2 (5\cos^2 i - 1) \tag{10}$$

$$\dot{\Omega} = -\frac{3}{2}J_2 n\left(\frac{R_e}{p}\right)^2 \cos i \tag{11}$$

where $n = \sqrt{\mu/a^3}$ is the mean motion, and $p = a(1-e^2)$ is the semilatus rectum. Note that the remaining mean elements a, e, and i are constant.

Roscoe et al. [8] suggested a new form for the along-track drift condition [Eq. (7)] to account for the fact that, since the ROI is only defined as a small portion of the orbit, better results could be obtained by minimizing the drift only in the ROI. For small $\delta\Omega_j$ and δi_j, the condition to negate the instantaneous along-track drift rate at some point in the orbit is

$$\delta\dot{f}_j + \delta\dot{\omega}_j + \delta\dot{\Omega}_j \cos i = 0 \tag{12}$$

and without J_2, the relationship between $\delta\dot{f}$ and $\delta\dot{M}$ is

$$\delta\dot{f} = \frac{\delta\dot{M}}{\eta^3}(1 + e\cos f)^2 \tag{13}$$

which suggests a modified along-track drift condition of the form

$$\delta\dot{M}_j + k_j(\delta\dot{\omega}_j + \delta\dot{\Omega}_j \cos i) = 0 \tag{14}$$

where k_j is a parameter defining the relative weighting of the mean motion to the differential argument of perigee and nodal precession rates. Taking the first variations of Eqs. (9–11) and substituting into Eq. (14) yields the modified δa_j condition

$$\delta a_j = \frac{J_2 R_e^2 (3\eta + 4k_j)}{2a\eta^4}\left[(3\cos^2 i - 1)\frac{e\delta e_j}{\eta^2} - \sin 2i\ \delta i_j\right] \tag{15}$$

The best performance for MMS is obtained for k_j values of approximately three (see discussion in [8]). For brevity in later sections, the leading coefficient on the right-hand side (RHS) of Eq. (15) is defined as C_j:

$$C_j = \frac{J_2 R_e^2 (3\eta + 4k_j)}{2a\eta^4} \tag{16}$$

B. Quality Factor

The MMS quality factor Q is a metric that determines, at a particular instant in time, the usefulness of the size and shape of the tetrahedron formed by the four MMS spacecraft. The quality factor is broken down into two subfunctions: Q_v that measures the quality of the shape of the tetrahedron and Q_s that measures the quality of the size of the tetrahedron [2].

The volumetric performance metric for MMS is defined as the ratio of the actual tetrahedron volume V_a to the volume of a regular tetrahedron with side lengths equal to the average side length of the actual tetrahedron V_r [17,18]:

$$Q_v = \frac{V_a}{V_r} = \frac{\sqrt{2}}{\bar{L}^3}|\mathbf{r}_1 \cdot (\mathbf{r}_2 \times \mathbf{r}_3)| \tag{17}$$

$\bar{L}$ is the average side length of the tetrahedron, and the vectors $\mathbf{r}_j$ are the positions of the three deputies relative to the chief. This metric has the useful property: $0 \le Q_v \le 1$. However, it does not take into account the actual size of the tetrahedron. Q_v will be equal to 1 when the volume of the tetrahedron equals that of a regular tetrahedron, and it will be equal to 0 when all four satellites lie in a plane.

A simple polynomial function is used as the size performance metric for MMS [2]:

$$Q_s(\bar{L}) = \begin{cases} 0 & \bar{L} < \ell_1 \\ \frac{(\bar{L}-\ell_1)^2(\bar{L}+\ell_1-2\ell_2)^2}{(\ell_2-\ell_1)^4} & \ell_1 \le \bar{L} < \ell_2 \\ 1 & \ell_2 \le \bar{L} \le \ell_3 \\ \frac{(\bar{L}-\ell_4)^2(\bar{L}-2\ell_3+\ell_4)^2}{(\ell_4-\ell_3)^4} & \ell_3 < \bar{L} \le \ell_4 \\ 0 & \bar{L} > \ell_4 \end{cases} \tag{18}$$

The constants ℓ_1, ℓ_2, ℓ_3, and ℓ_4 are used to change the shape of the function and are prescribed for the various formation sizes of interest for MMS. The important properties of this metric are that it will be equal to 1 when the formation is within a desired size range (based on its average side length), it will be equal to 0 when the formation size is unacceptable (either too large or too small), and it will vary continuously between 0 and 1 in the intermediate range.

The MMS quality factor is defined as the product of the volumetric performance metric and the size performance metric

$$Q = Q_v Q_s = \frac{\sqrt{2}Q_s}{\bar{L}^3}|\mathbf{r}_1 \cdot (\mathbf{r}_2 \times \mathbf{r}_3)| \tag{19}$$

The average quality factor in the ROI is

$$\bar{Q}_{\text{ROI}} = \frac{1}{t_2 - t_1}\int_{t_1}^{t_2} Q\,\mathrm{d}t \tag{20}$$

where t_1 and t_2 are the times at which the formation enters and exits the ROI, respectively. The integration is to be discretized with respect to true anomaly; therefore, Eq. (20) is rewritten in terms of f:

$$\bar{Q}_{\text{ROI}} = \frac{\eta^3}{M_2 - M_1}\int_{f_1}^{f_2} \frac{Q\,\mathrm{d}f}{(1 + e\cos f)^2} \tag{21}$$

Discretizing at N_f equal spacings of true anomaly,

$$\bar{Q}_{\text{ROI}} \approx \frac{\eta^3}{N_f}\frac{f_2 - f_1}{M_2 - M_1}\sum_{k=1}^{N_f}\frac{Q_k}{(1 + e\cos f_k)^2} \tag{22}$$

The MMS mission requirements call for a quality factor that exceeds 0.7 for 80% of the time in the ROI. A good approximation to the quality factor requirement is that $\bar{Q}_{\text{ROI}}$ exceeds 0.78,[¶] and it is this condition that will be used throughout the rest of this paper to determine whether or not a given formation is satisfactory. In addition, a requirement is imposed such that the minimum separation distance between any pair of satellites $d_{\min}$ must be greater than 6 km at all times: this is slightly more conservative than the actual mission requirement of 4 km at all times and 6 km near perigee.

C. Formation Optimization

For the initial formation optimization of MMS, the cost function is chosen to be the negative of the average quality factor in the ROI

$$J = -\bar{Q}_{\text{ROI}} \tag{23}$$

Two optimization processes were defined by Roscoe et al. [8]: the single-orbit constrained (SOC) optimization and the multiorbit

[¶]Personal communications with Steven P. Hughes, NASA Goddard Space Flight Center, Greenbelt, MD, 17 March 2010.

unconstrained (MOU) optimization. The SOC optimization problem is defined as

$$\begin{aligned} &\text{minimize} && \text{J} \\ &\text{with respect to} && \delta\mathbf{e}_j, \qquad j = 1, 2, 3 \\ &\text{subject to} && \delta a_j = C_j \left[(3\cos^2 i - 1)\frac{e\delta e_j}{\eta^2} - \sin 2i\ \delta i_j \right] \end{aligned}$$

in which the performance of the formation is maximized over one orbit, subject to the modified along-track drift condition of Eq. (14). The MOU optimization problem is defined as

$$\begin{aligned} &\text{minimize} && \sum_{k=1}^{N_{\text{orb}}} J_k \\ &\text{with respect to} && \delta\mathbf{e}_j, \qquad j = 1, 2, 3 \end{aligned}$$

where J_k is the cost in the kth orbit and N_{orb} is the total number of orbits to be considered. This optimization is designed to achieve long-term stability of the tetrahedron configuration without using the δa_j constraint. The MOU optimization produces slightly better long-term results but at a much greater cost in terms of computation requirements.

D. Quantification of Errors

Hughes [3] performed an extensive error sensitivity analysis for the MMS mission. Error sources (including maneuver magnitude, direction, and timing as well as navigation) were evaluated by comparing the resulting differential semimajor axis errors. Since long-term stability is the primary focus of this paper, examining only errors in δa is reasonable since their effect on formation stability is $\mathcal{O}(1)$, whereas the effect of any of the other elements is $\mathcal{O}(J_2)$ or higher.

According to the statistical model described by Hughes [3], δa errors due to maneuver magnitude errors are distributed normally with a mean of 0 and a standard deviation σ of about 17 m. Errors due to maneuver direction errors are distributed normally with $\sigma \approx 3$ m. The worst-case maneuver timing error results in a δa error of about 4 m, and navigation errors result in δa errors normally distributed with $\sigma \approx 1$ m (for Phase I). To account for all of these error sources, in this paper, a slightly conservative estimate of $3\sigma = 80$ m is used for the distribution of δa errors.

III. Performance in Presence of Errors

To measure the performance of a given formation in the presence of δa errors, the quantity T is defined as the number of days (one orbit $\approx$ one day) that a formation satisfies the MMS mission requirements ($\bar{Q}_{\text{ROI}} \geq 0.78$ and $d_{\min} > 6$ km). The distribution of T values resulting from the expected δa error distribution will determine the performance of a given formation design. In particular, it is desired that the formation has a high mean T and a high probability that T will be greater than 14 days.

The results of performing Monte Carlo analyses on the 10 km SOC (with $k_j = 3$), 60-orbit MOU, and 90-orbit MOU optimized formations derived by Roscoe et al. [8] are summarized in Table 1. However, since the initial SOC and MOU optimizations for the 10 km formations generally result in initial separation distances of about 5 km, only quality factor performance is considered here, and no minimum separation requirement is imposed. Each set of results was obtained by sampling a $3\sigma = 80$ m normal distribution for the δa error of each deputy, using Latin hypercube sampling, and running 5000 simulations in MATLAB to calculate the T distribution. The quantities listed are the minimum $T_{\min}$, maximum $T_{\max}$, and mean time $\bar{T}$ to $\bar{Q}_{\text{ROI}} < 0.78$, and the probability that T is less than or equal to 14 days, $P_T(T \leq 14)$. The note "peak" means that the location of the maximum $\bar{Q}_{\text{ROI}}$ has been shifted to the indicated orbit number, since the MOU optimization generally produces solutions in which the maximum $\bar{Q}_{\text{ROI}}$ does not occur on the first orbit (see discussion in [8]).

Table 1 Monte Carlo results for 10 km SOC and MOU optimizations

Optimization	$T_{\min}$	$T_{\max}$	$\bar{T}$	$P_T(T \leq 14)$
SOC	7	66	26.8	0.085
MOU 60 orbit	7	97	30.6	0.082
MOU 60 orbit (peak 22)	7	86	27.8	0.118
MOU 60 orbit (peak 0)	7	68	25.5	0.143
MOU 90 orbit	5	110	27.5	0.202
MOU 90 orbit (peak 26)	6	89	27.9	0.130
MOU 90 orbit (peak 0)	7	71	25.2	0.162

In the absence of errors, the 10 km SOC, 60-orbit MOU, and 90-orbit MOU optimized formations satisfy the quality factor requirement for 65, 95, and 110 days, respectively. However, the performance of these formations is quite poor in the presence of errors, without even considering the additional minimum separation distance requirement. Examining Fig. 4a, which shows a histogram of the T distribution for the 60-orbit MOU case, it is clear that very few of the cases are in the vicinity of the ideal result, and most of them have much lower T values. Similarly, in Figs. 5a–5c, which show the distribution of T with respect to the δa errors of the deputies, the majority of the data are concentrated at the base of the distribution, with very few near the narrow peak. The same behavior was observed in each of the Monte Carlo simulations listed in Table 1.

The larger formation sizes perform better in the presence of errors than do the 10 km ones. The results of performing Monte Carlo analyses on the remaining MMS Phase I formation sizes, including the minimum separation requirement, are summarized in Table 2 for the 60-orbit MOU optimized formations derived by Roscoe et al. [8]. The results for the 60 and 160 km formations are very good, considering that the total time MMS Phase I will spend in these formations is 15 days each. The results for the 25 km formation are adequate but could be improved, especially in the lower limit. Figure 4b shows a histogram of the T distribution for this case, in which a large portion of the data are located near the higher end of the distribution, with a fairly wide base extending toward the lower end.

According to Roscoe et al. [8], the size of the desired tetrahedron does not significantly affect the quality factor evolution of the optimized formation designs for MMS, since nonlinear effects in the dynamics are very small compared with J_2 and other perturbations. In fact, in that paper, the 60-orbit MOU optimization results were observed to be virtually identical for all of the Phase I formation sizes considered. Why, then, does formation size have a significant effect on the Monte Carlo analysis performed in this section?

There are two reasons: first, the minimum separation distance requirement and, second, the scaling of the formation size parameters. Since the $d_{\min}$ requirement is stated as an absolute distance (6 km), it will have much more of an effect on small formations sizes than on larger ones. In the analysis of the 10 km formations, this requirement was not even included, because all of the formation designs would have failed on the first orbit. For the 25 km formations, this requirement has some effect, producing several of the lower values of T in the distribution but only for certain combinations of the deputy δa errors. The 60 and 160 km formations are completely unaffected by this requirement.

The effect of scaling the formation size parameters can be best illustrated by way of a simple example. Consider the total drift in position per orbit ρ_d, resulting from a δa error for a single deputy in an unperturbed reference orbit [19]

$$\rho_d = \delta a \frac{3\pi}{\eta}\sqrt{1 + e^2 + 2e\cos f_0} \tag{24}$$

where f_0 is the true anomaly being considered, since in an eccentric reference orbit, the drift will be different at different points in the orbit. The drift rate depends only on δa and not on the distance between the satellites. Therefore, a small formation will experience the same amount of drift as a larger one, although the drift will seem much larger when compared with the actual formation size. Additionally, the Q_s side length parameters, ℓ_1–ℓ_4, scale with formation

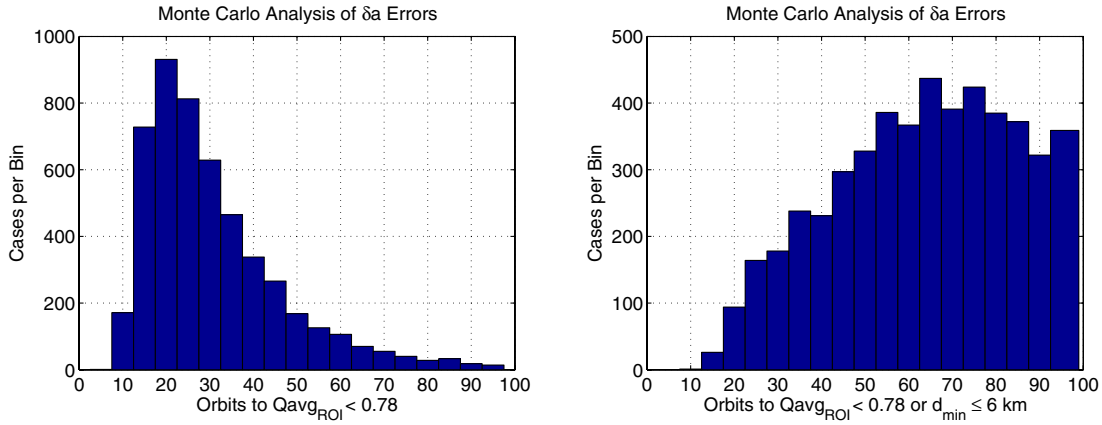

a) 10 km formation **b) 25 km formation**

Fig. 4 Effect of $3\sigma = 80$ m δa errors in each deputy on the 60-orbit MOU optimization.

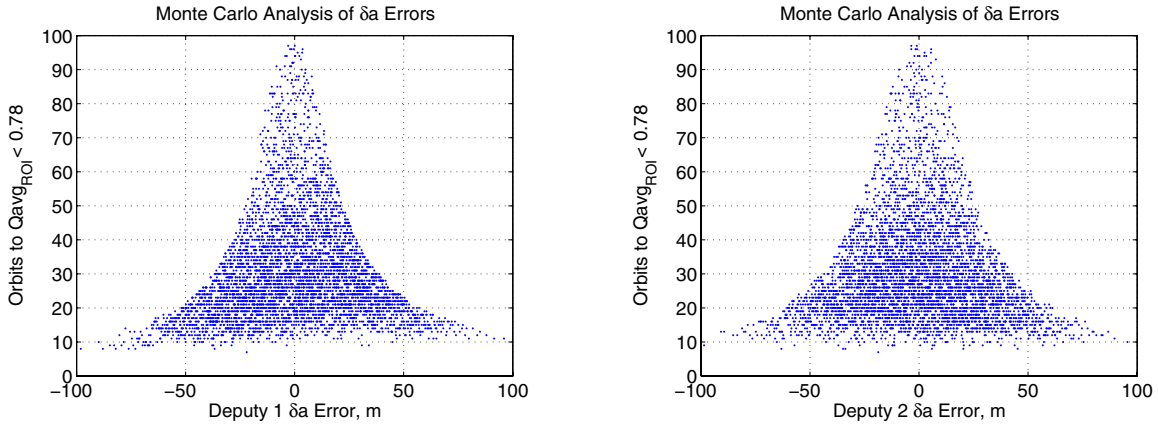

a) Deputy 1 **b) Deputy 2**

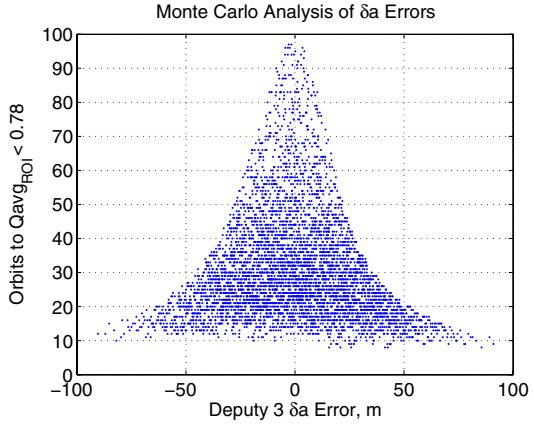

c) Deputy 3

Fig. 5 T distribution for $3\sigma = 80$ m δa errors applied to 60-orbit MOU optimization.

Table 2 Monte Carlo results for 60-orbit MOU optimizations

Formation size	$T_{\min}$	$T_{\max}$	$\bar{T}$	$P_T(T \leq 14)$
25 km	12	99	63.1	0.001
60 km	36	98	85.0	0
160 km	73	95	87.3	0

size and are consequently spaced farther apart for larger formations, and the average side length appears in the denominator of Q_v [Eq. (17)], thus tolerating greater absolute variations in side length throughout the ROI. It can then be concluded that a given δa error will have a greater effect on the quality factor of a small formation than it will on a larger one (not considering nonlinear effects) and, in general, the smaller formation sizes can be expected to fail the quality factor requirement sooner than the larger ones when considering the same error magnitudes.

Table 3 MMS reference mean orbital elements

Property	Value
a, km	42,095
e	0.81818
i, °	28.5
Ω, °	357.857
ω, °	298.2253
M_0, °	180

Table 4 Monte Carlo results for 10 km robust optimizations

Initial design	N_{orb}	$T_{\min}$	$T_{\max}$	$\bar{T}$	$P_T(T \leq 14)$
SOC	60	8	83	42.4	0.034
MOU 60 orbit	60	9	82	44.7	0.015
MOU 90 orbit	60	8	85	41.1	0.034
SOC	40	10	75	45.6	0.005
SOC	30	12	77	44.2	0.004
MOU 60 orbit	30	9	73	43.9	0.018
MOU 90 orbit	30	11	80	42.7	0.006
SOC	20	11	73	43.3	0.003
SOC	10	11	68	41.9	0.002

IV. Robust Optimization

To obtain better performance in the presence of errors for the 10 and 25 km formations, a new cost function must be defined to allow for a tradeoff between maximum performance and robustness. Because of the logistical time and effort required to reconfigure the formation, the cost function must also emphasize worst-case performance in order to reduce the probability of having to maneuver the satellites too frequently (defined as 14 days or less for MMS). Therefore, a stochastic approach is used, as suggested by de Pauw et al. [20].

The expectation value for $\bar{Q}_{\text{ROI}}$, given the probability density function (PDF) $P(\delta\mathbf{a}_e)$ of the three deputies' δa errors, is

$$E(\bar{Q}_{\text{ROI}}) = \int_{-\infty}^{\infty}\int_{-\infty}^{\infty}\int_{-\infty}^{\infty} \bar{Q}_{\text{ROI}} P(\delta\mathbf{a}_e)\, \mathrm{d}\delta\mathbf{a}_e \tag{25}$$

where $\delta\mathbf{a}_e$ is defined as

$$\delta\mathbf{a}_e = [\,\delta a_{e1} \quad \delta a_{e2} \quad \delta a_{e3}\,]^T \tag{26}$$

A crude approximation to this value can be made by discretizing at N_1, N_2, and N_3 points of δa_{e1}, δa_{e2}, and δa_{e3}, respectively:

$$E^*(\bar{Q}_{\text{ROI}}) = \frac{1}{N_1 N_2 N_3}\sum_1\sum_2\sum_3 \bar{Q}_{\text{ROI}} P(\delta\mathbf{a}_e) \tag{27}$$

It is worth noting that, for this to be a proper approximation, there should be a another term multiplying the RHS of Eq. (27) related to the range of δa errors being sampled. However, omitting this term will not make a difference in the result, since it is constant with respect to the optimization that will be defined shortly.

According to the error model described in Sec. II.D, the distribution of each deputy δa error can be described by a normal PDF with mean 0 and standard deviation σ. Therefore, their combined PDF can be written

$$P(\delta\mathbf{a}_e) = \frac{1}{\sqrt{(2\pi)^3\sigma^2}}\exp\left[-\frac{\delta\mathbf{a}_e^T\delta\mathbf{a}_e}{2\sigma^2}\right] \tag{28}$$

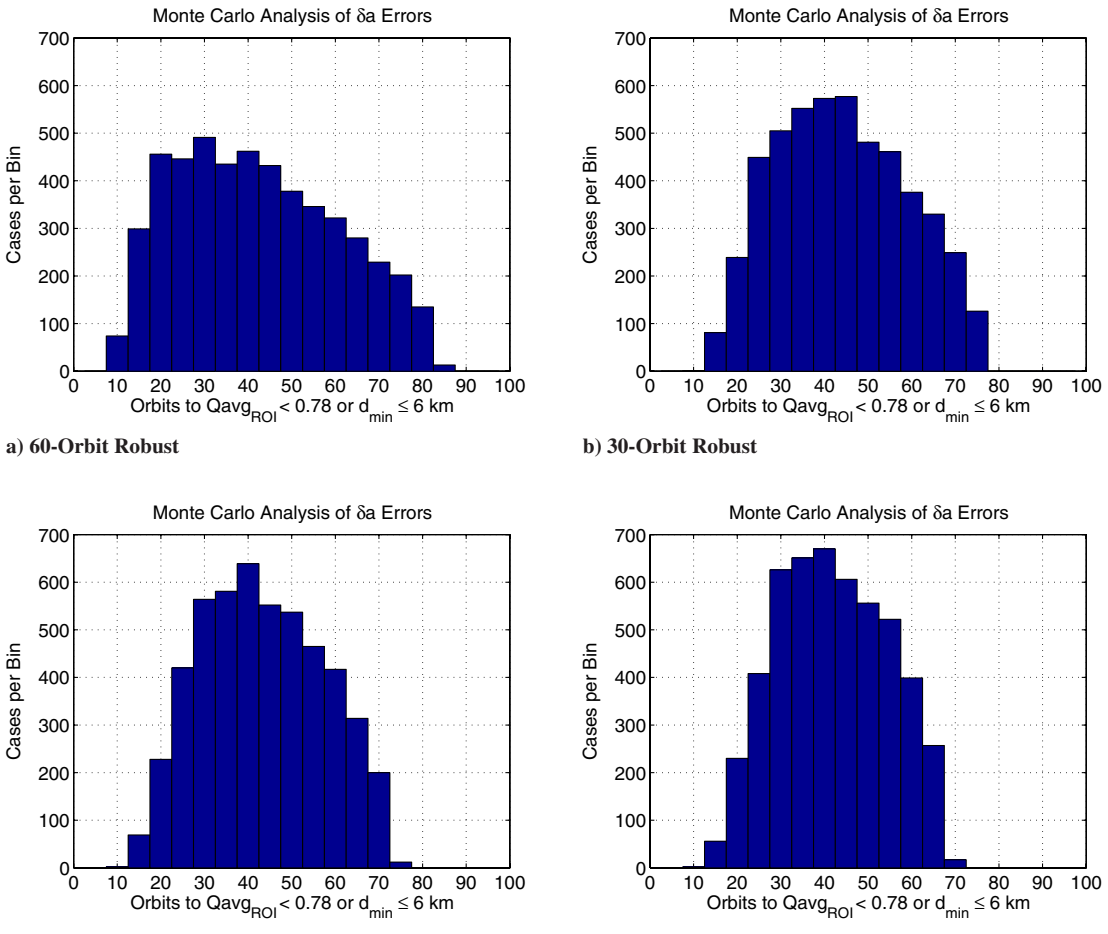

Fig. 6 Effect of $3\sigma = 80$ m δa errors on robust optimization of the 10 km SOC result.

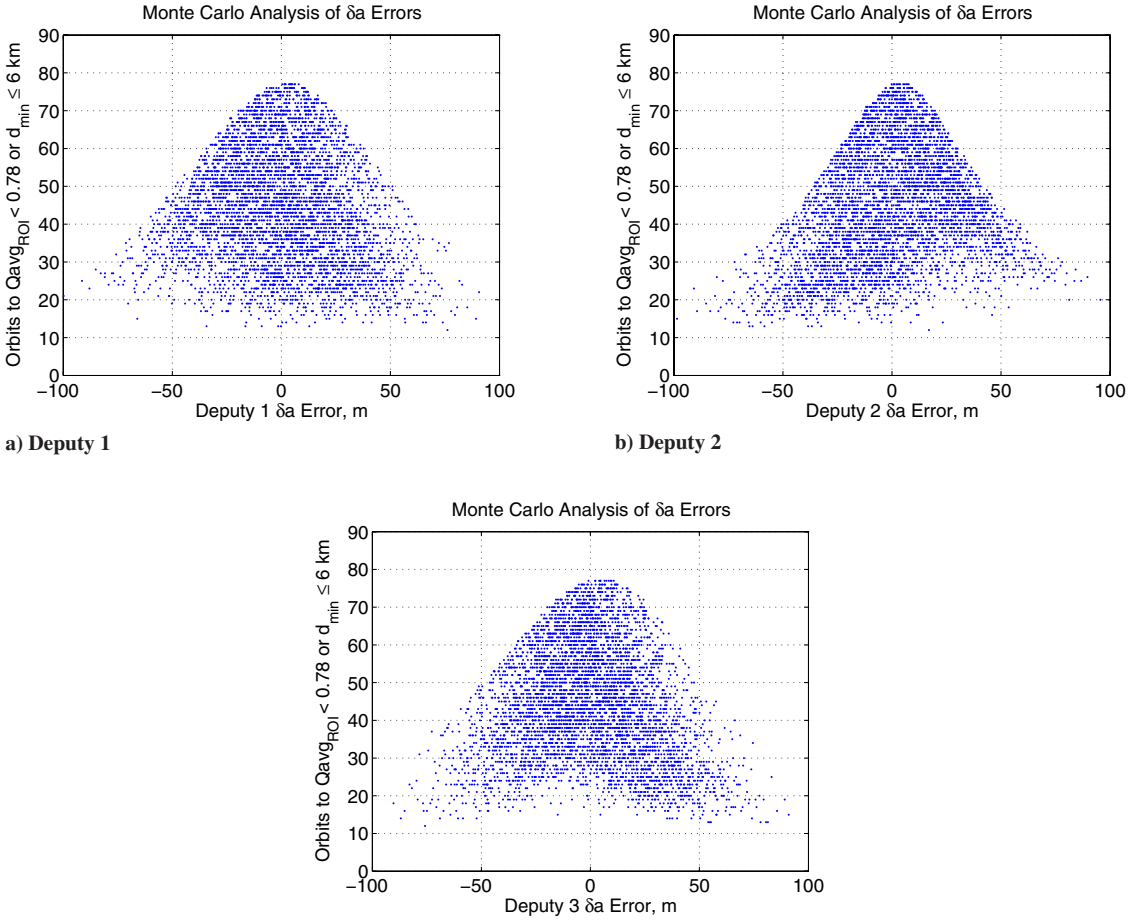

a) Deputy 1 **b) Deputy 2** **c) Deputy 3**

Fig. 7 T distribution for $3\sigma = 80$ m δa errors applied to the 10 km, 30-orbit robust SOC result.

since the errors are independent and σ is the same for each deputy. The robust cost function is defined by substituting Eq. (28) into Eq. (27), negating it, and sampling at N points for each deputy:

$$J_r^* = -\frac{1}{N^3}\sum_{i=1}^{N^3} \bar{Q}_{\mathrm{ROI},i} \exp\left[-\frac{\delta\mathbf{a}_{e,i}^T \delta\mathbf{a}_{e,i}}{2\sigma^2}\right] \tag{29}$$

where the leading coefficient on the RHS of Eq. (28) has been omitted. Furthermore, an additional parameter w can be included in Eq. (29) to tune the relative weighting of each point in the computation of the overall cost, yielding the final form of the cost function

$$J_r = -\frac{1}{N^3}\sum_{i=1}^{N^3} \bar{Q}_{\mathrm{ROI},i} \exp\left[-\frac{\delta\mathbf{a}_{e,i}^T \delta\mathbf{a}_{e,i}}{2\sigma^2 w}\right] \tag{30}$$

The tuning parameter w must be positive and is used to directly control the tradeoff between maximum performance and robustness: $w = 1$ corresponds to maximizing the approximate expectation value given in Eq. (27), $w = \infty$ corresponds to equal weighting of all sample points (a uniform PDF), $0 < w < 1$ places more emphasis on sample points near the center of the distribution (maximum performance), and $1 < w < \infty$ places more emphasis on sample points near the tails of the distribution (robustness).

The robust optimization problem is then defined as

$$\begin{aligned} &\text{minimize} && \sum_{k=1}^{N_{\mathrm{orb}}} J_{r,k} \\ &\text{with respect to} && \delta\mathbf{e}_{\mathrm{nom},j}, \qquad j = 1,2,3 \\ &\text{subject to} && \delta a_{\mathrm{nom},j} = C_j\left[(3\cos^2 i - 1)\frac{e\delta e_j}{\eta^2} - \sin 2i\delta i_j\right] \end{aligned}$$

where $\delta a_{\mathrm{nom},j}$ is the nominal or target δa_j given by the modified along-track drift condition defined in Sec. II.A. Similarly, $\delta\mathbf{e}_{\mathrm{nom},j}$ are the nominal differential orbital elements; however, no errors are being applied to any elements except for δa_j. Since $\delta a_{\mathrm{nom},j}$ is explicitly specified by the along-track drift condition, the design variables are essentially the remaining $5 \times 3 = 15$ differential elements of the deputies. The optimization is performed over multiple

Table 5 Robust optimized differential mean orbital elements from SOC initial design

	10 km, 30-orbit robust			25 km, 40-orbit robust		
	1	2	3	1	2	3
δa, m	−40.175	−52.664	−40.977	−90.335	−72.019	−83.197
δe, 10^{-4}°	−1.944	−2.528	−1.629	−4.436	−3.669	−3.438
δi, 10^{-3}°	−1.593	−1.636	6.257	−5.024	−6.949	9.801
$\delta\Omega$, 10^{-2}°	−0.201	−0.109	1.350	−0.534	−0.119	1.997
$\delta\omega$, 10^{-2}°	−0.950	1.031	−1.275	−0.172	2.962	−0.545
δM_0, 10^{-2}°	2.838	−2.553	−0.014	1.115	−8.748	−4.245

Table 6 Monte Carlo results for 25 km robust optimizations

Initial design	N_{orb}	T_{min}	T_{max}	$\bar{T}$	$P_T(T \leq 14)$
SOC	60	12	87	65.0	0.000
MOU 60 orbit	60	24	87	68.2	0
SOC	40	27	79	63.2	0
SOC	30	25	75	60.7	0

Table 7 GMAT Monte Carlo results for robust optimizations

Initial design	N_{orb}	T_{min}	T_{max}	$\bar{T}$	$P_T(T \leq 14)$
			10 km		
SOC	30	11	66	39.8	0.008
MOU 60 orbit	30	10	65	37.7	0.018
MOU 90 orbit	30	12	69	38.5	0.005
			25 km		
SOC	40	26	67	48.6	0

orbits, since long-term formation stability is the primary goal of this process.

Qualitatively, this robust optimization process attempts to improve performance in the presence of errors by sampling the error distribution at several points for each deputy, computing the effect on the quality factor of each combination of errors, and creating a new performance index, which is the sum of the old performance indices, for each combination of errors, weighted by some function of their probabilities.

V. Robust Performance in Presence of Errors

The robust optimization scheme is implemented by first performing either an SOC or MOU optimization, and then using that design as the initial guess for the robust optimizer. The δa error distribution is sampled at three points for each deputy, -3σ, 0, and 3σ, and a tuning parameter w of 9 was selected based on the results of several test cases. The initial mean elements of the MMS Phase I reference orbit are listed in Table 3. For the 10 km formation size, some care had to be taken in generating the initial guess for the robust optimization in order to ensure acceptable performance in terms of the d_{min} requirement. As mentioned in Sec. III, the 10 km formation optimizations generally produce results with initial side lengths of about 5 km, which is unacceptable. However, there is some flexibility in the range of possible side lengths provided by the definition of Q_s. The side length parameters for the 10 km formation are $\ell_1 = 4$ km, $\ell_2 = 6$ km, $\ell_3 = 18$ km, and $\ell_4 = 25$ km; it was found that selecting an initial tetrahedron for the SOC optimization with sides of 18 km (instead of 10 km) converged to a solution with an initial side length of about 13 km, which then produced better results in the robust optimization process.

The results of Monte Carlo simulations for several different robust optimizations of the 10 km formation for MMS Phase I are listed in Table 4, with the minimum separation requirement enforced. In each Monte Carlo simulation, 5000 cases were considered, with δa errors generated in the same manner as was described in Sec. III. All of the robust optimized formations exhibit better overall behavior in the presence of δa errors than did those of the previous analyses (in Sec. III). In general, the robust optimization process produces narrower and more even histograms of the formation lifetime T at a cost of some degradation in performance near the ideal case, as was expected. There are small differences between using the SOC or MOU optimizations to provide the initial guess, but the SOC method (with $k_j = 3$) produces acceptable results at a fraction of the computation time of the MOU method. The effect of varying N_{orb} in the robust optimization can be seen in Figs. 6a–6d: lowering N_{orb} essentially narrows the histogram and increases the likelihood that the data will be near the mean value. Figures 7a–7c show the distribution of T with respect to the δa errors of the deputies, which clearly shows an improvement over the 10 km formation results of Sec. III (which did not include the d_{min} requirement). The classical initial differential mean orbital elements for the 30-orbit robust optimization of the 10 km SOC formation are listed in Table 5.

The results of Monte Carlo simulations for the robust optimization of the 25 km formation are listed in Table 6. As was the case with the 10 km simulations, there is a marked improvement over the non-robust performance. In Figs. 8a and 8b, the same narrowing of the histogram is evident as N_{orb} gets smaller, although there is little effect when it is decreased below 40 orbits. The classical initial differential mean orbital elements for the 25 km, 40-orbit robust optimization are listed in Table 5.

VI. NASA General Mission Analysis Tool Verification

The G–A STM is accurate for small satellite separations and contains terms up to the first order in J_2. Because of the high eccentricity of the reference orbit and the long duration of the mission, it is expected that the accuracy of the predicted motion of the satellites will degrade after a certain amount of time. The results of Roscoe et al. [8] indicate that nonlinear effects are not significant for any of the formation sizes considered in the Phase I analysis (up to 160 km); therefore, the main inaccuracies in the results are expected to come from other sources. Four of the robust optimized formation designs described in the previous section were verified using the GMAT. For each one, 1000 cases were simulated with δa errors using a fourth-degree fourth-order gravity model, along with the solar and lunar gravity perturbations, and the solar radiation pressure. Only 1000 cases were simulated in GMAT, compared with 5000 cases in MATLAB, because of the significantly longer simulation time it required.

Table 7 lists results for the GMAT Monte Carlo simulations of the 10 km, 30-orbit robust optimized formations for the SOC, 60-orbit MOU, and 90-orbit MOU initial designs. Comparing these results

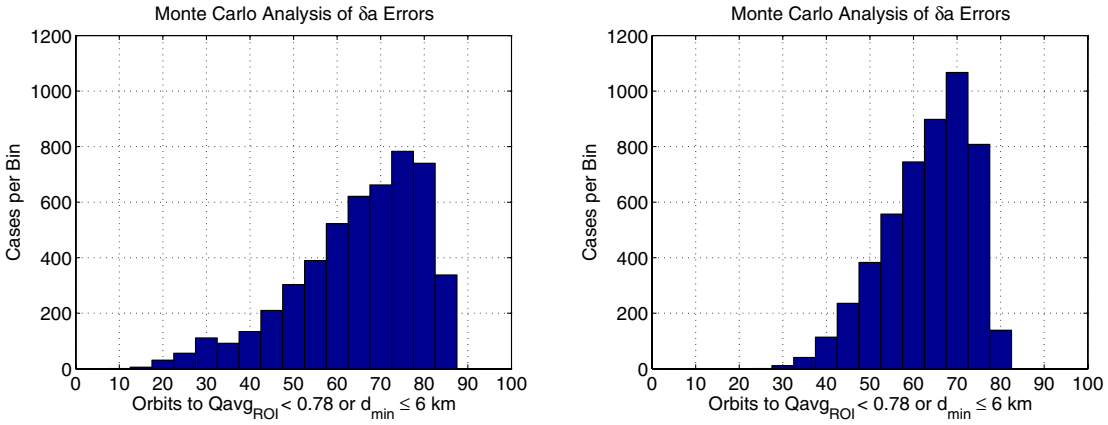

a) 60-Orbit Robust **b) 40-Orbit Robust**

Fig. 8 Effect of $3\sigma = 80$ m δa errors on the 25 km, robust optimization of the SOC result.

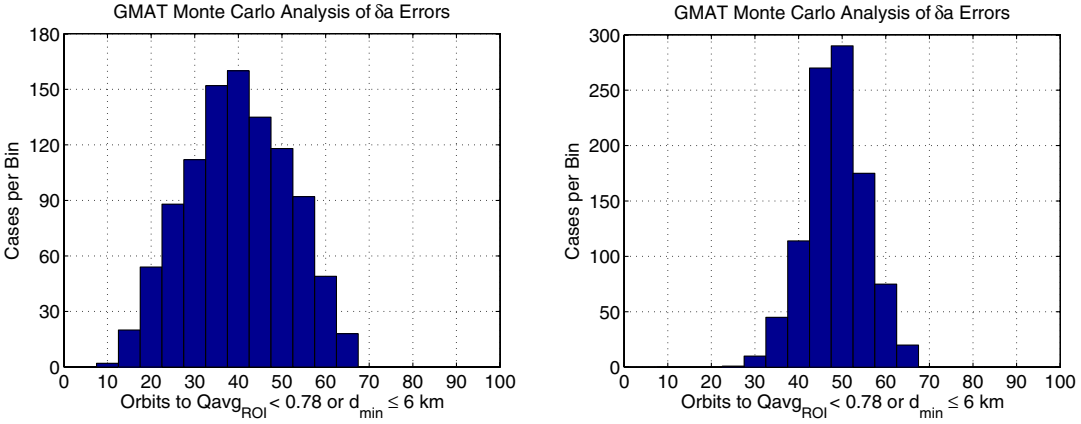

a) 10 km, 30-Orbit Robust from SOC **b) 25 km, 40-Orbit Robust from SOC**

Fig. 9 Effect of $3\sigma = 80$ m δa errors on robust optimizations, simulated in GMAT.

with those of Table 4, it is clear that the GMAT results generally predict a shorter maximum formation lifetime than do the G–A STM ones, consequently lowering the mean T value as well. This is consistent with the observations of Roscoe et al. [8], who found the G–A STM predictions to be reasonably accurate up to about 70 days. A histogram of the T distribution for the robust optimized SOC result is shown in Fig. 9a. Comparing this to Fig. 6b, there is good agreement in the lower end of the distribution, with a much higher peak at about 40 orbits, after which the GMAT results fall off more quickly, as expected.

The results for the 25 km, 40-orbit robust optimized SOC formation are listed in Table 7, and a histogram is plotted in Fig. 9b. As was the case with the 10 km results, there is good agreement with the G–A STM results of Fig. 8b at the lower end of the distribution, a higher peak near the GMAT mean, and lower values for the upper end of the distribution.

VII. Physical Significance

In this section, the physics of the MMS formation are examined, including the effects of the robust optimization. Figure 10 shows the apogee formation geometry (in the LVLH frame) resulting from several different design methods. Each design method is examined during the orbit of the peak average quality factor (as previously mentioned, most multiorbit designs do not have their maximum $\bar{Q}_{\text{ROI}}$ on the first orbit). In each case, three of the satellites are roughly in the plane of the reference orbit, forming the base of the tetrahedron, and the fourth is out of the plane. According to the orbital elements listed in Table 5, the out-of-plane deputy's displacement is created by a combination of both differential inclination and right ascension (in both cases, satellite 3 is the out-of-plane deputy). In all of the designs, especially the longer-term ones (larger N_{orb} in the optimizations), the bases of the tetrahedra are not quite aligned with the plane of the reference orbit; this is caused by long-term secular effects due to J_2 (since later orbits are being observed in these cases).

It is interesting that the robust optimizations produced larger overall formations (about 14 km at apogee) than did the nonrobust SOC or MOU optimizations, even though no minimum separation constraint was imposed in the design process. The increase in size could be due to the definition of Q_v [Eq. (17)]; since $\bar{L}$ appears in the denominator, increasing the overall formation size makes Q_v less sensitive to a given δa error magnitude. The larger size also results in larger values of the nominal δa: about 40–50 m for the 10 km formation, according to Table 5, compared with about 10–20 m for the nonrobust result (listed in [8]).

To better understand the geometries of the optimal tetrahedra and to investigate possible symmetries in the solutions, 500 random initial formations were generated [by choosing 500 random values of the tetrahedron orientation angles ϕ, ψ, and γ, defined in Eq. (1)] and optimized using the 60-orbit MOU method. The nominal formation lifetimes were measured and, aside from a few small clusters of lower values, were found to range from 90–95 days with a mode of 94. The geometries of the best formations, with lifetimes of 95 days, were examined, and from these results were identified eight possible tetrahedron orientations, which are shown in Fig. 11 (the four solid tetrahedra are above the orbit plane, and the four dashed tetrahedra are below the orbit plane). In fact, these can really be considered two possible orientations, in which the chief satellite can be placed at any

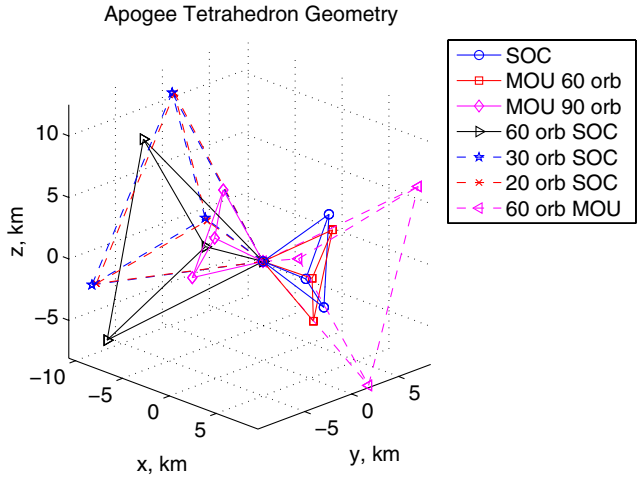

Fig. 10 10 km formation configuration at apogee (rob denotes robust; orb denotes orbit).

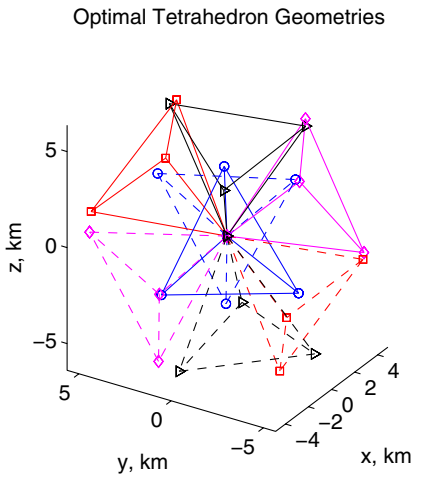

Fig. 11 Possible optimal formation configurations (10 km).

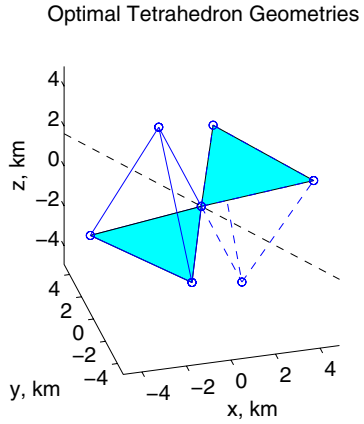

Fig. 12 Pair of optimal formation configurations (10 km).

of the four vertices to give a total of eight configurations. Each of the tetrahedra has a base that lies roughly in the plane of the reference orbit, and one satellite is out of the plane. Pairs of orientations do not have a plane of symmetry, but they are related by a 180° rotation about a line in the x-y plane, parallel to the side of the base furthest from the origin, as shown in Fig. 12. In each case, the base is slightly inclined with respect to the reference orbit, most likely to account for J_2, which will cause it to precess over the course of the mission.

Figures 13a–13e illustrate how the tetrahedron evolves throughout the ROI, and Fig. 13f shows the formation at perigee. Projected onto the orbit plane, the motion of the deputies is elliptical, each with its own phase. As a whole, the tetrahedron slowly revolves about the z axis, contracting and growing taller until it reaches apogee, and then expanding symmetrically. The formation forms a regular tetrahedron at two points (in Figs. 13b and 13d), which correspond to the peaks of the quality factor (shown in Fig. 14a). Outside the ROI, the tetrahedron continues to revolve but distorts as it nears perigee; the deputy with the large out-of-plane displacement crosses briefly through the base of the tetrahedron as the formation passes through this point.

Figures 14a and 14b show the quality factor and average quality factor for several different formation design methods. Figure 14a shows the instantaneous quality factor over the orbit corresponding to the maximum $\bar{Q}_{\mathrm{ROI}}$ for each case, and the vertical lines indicate the location of the ROI. The main distinguishing characteristic of the robust optimized results is that they produce a narrower peak in the quality factor curve than do the other optimizations. The times of Figs. 13a–13e refer to, respectively, the beginning of the ROI, the first peak of the quality factor, the apogee, the second peak of the quality factor, and the end of the ROI. Figure 14b shows that the average quality factors for the robust optimizations do not quite reach the maxima of either the SOC or 60-orbit MOU optimizations, and they fall off more steeply as well, illustrating the fact that some performance has been sacrificed in the error-free case to gain a more robust formation design.

VIII. Conclusions

A new design method is proposed for spacecraft formations using a robust optimization approach based on maximizing a weighted sum of the offnominal mean quality factor subject to differential semimajor axis δa errors. In this paper, only δa errors are considered, but the theory can be extended to include additional error sources as well. The modified along-track drift condition proposed by Roscoe et al. [8] is used to enforce long-term stability of the nominal formation, and it is shown to produce high mean formation lifetimes in the offnominal cases as well. Statistical analyses of formation lifetimes were performed for the robust optimization method and nonrobust methods for Phase I of the Magnetospheric Multiscale Mission, and performance was shown to be much better in the presence of errors using the robust approach. Larger formations were also found to be less sensitive to a given magnitude of δa errors than were smaller formations. Results were verified in a higher-order gravity model with additional perturbations using the NASA General Mission Analysis Tool. All of the design methods produce optimal tetrahedra with three satellites roughly in the plane of the reference orbit and one largely out of the plane.

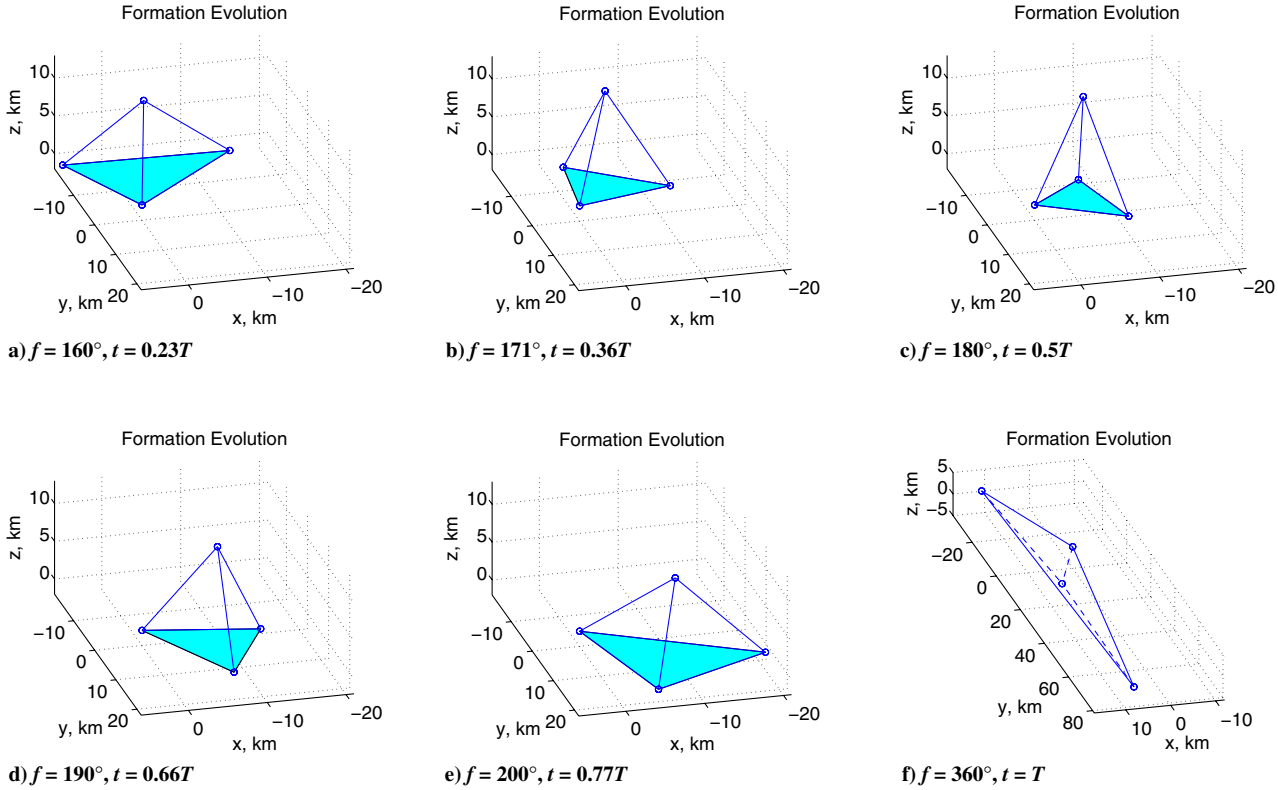

a) $f = 160°, t = 0.23T$ **b)** $f = 171°, t = 0.36T$ **c)** $f = 180°, t = 0.5T$

d) $f = 190°, t = 0.66T$ **e)** $f = 200°, t = 0.77T$ **f)** $f = 360°, t = T$

Fig. 13 Evolution of 30-orbit robust 10 km MMS tetrahedron formation.

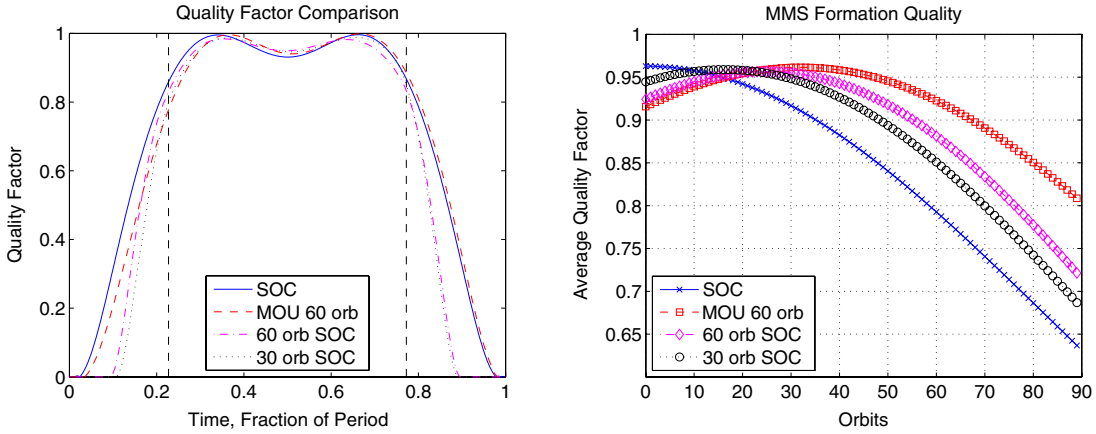

a) Quality factor **b) Average quality factor**

Fig. 14 Comparison of robust and nominal quality factor performances (rob denotes robust; orb denotes orbit).

Acknowledgments

The research reported in this paper has been supported by the NASA Goddard Space Flight Center under contract NNX10AB73G. The authors appreciate the technical input provided by Cheryl Gramling, Trevor Williams, Steven Hughes, and Conrad Schiff.

References

[1] Curtis, S., "The Magnetospheric Multiscale Mission... Resolving Fundamental Processes in Space Plasmas," NASA Science and Technology Definition Team for the MMS Mission, Rept. NASA/TM-2000-209883, 1999.

[2] Hughes, S. P., "General Method for Optimal Guidance of Spacecraft Formations," *Journal of Guidance, Control, and Dynamics*, Vol. 31, No. 2, March–April 2008, pp. 414–423. doi:10.2514/1.23731

[3] Hughes, S. P., "Formation Design and Sensitivity Analysis for the Magnetospheric Multiscale Mission (MMS)," AIAA/AAS Astrodynamics Specialist Conference, Honolulu, HI, AIAA Paper 2008-7357, Aug. 2008.

[4] Gim, D.-W., and Alfriend, K. T., "Criteria for Best Configuration and Sub-Optimal Reconfiguration for MMS Mission," *Advances in the Astronautical Sciences*, Vol. 119, 2004, pp. 947–968.

[5] Alfriend, K. T., and Yan, H., "An Orbital Elements Approach to the Nonlinear Formation Flying Problem," *Proceedings of the International Formation Flying Symposium*, Toulouse, France, Centre National d'Etudes Spatiales, Paris, Oct. 2002.

[6] Griffith, J. D., Singh, L., and How, J. P., "Optimal Microsatellite Cluster Design for Space-Based Tracking Missions," AIAA Guidance, Navigation and Control Conference and Exhibit, Hilton Head, SC, AIAA Paper 20078-6543Aug. 2007.

[7] Griffith, J. D., "Design and Control of Microsatellite Clusters for Tracking Missions," S.M. Thesis, Massachusetts Inst. of Technology, Cambridge, MA, May 2007.

[8] Roscoe, C. W. T., Vadali, S. R., and Alfriend, K. T., "Design of Satellite Formations in Orbits of High Eccentricity with Performance Constraints Specified Over a Region of Interest," *AAS/AIAA Kyle T. Alfriend Astrodynamics Symposium*, Monterey, CA, American Astronomical Soc. Paper 10-310, Washington, D.C., May 2010.

[9] Gim, D.-W., and Alfriend, K. T., "State Transition Matrix of Relative Motion for the Perturbed Noncircular Reference Orbit," *Journal of Guidance, Control, and Dynamics*, Vol. 26, No. 6, Nov.–Dec. 2003, pp. 956–971. doi:10.2514/2.6924

[10] Lawden, D. F., *Optimal Trajectories for Space Navigation*, Butterworths, London, 1963, pp. 79–86.

[11] Tschauner, J., "Elliptic Orbit Rendezvous," *AIAA Journal*, Vol. 5, No. 6, June 1967, pp. 1110–1113. doi:10.2514/3.4145

[12] Tschauner, J., and Hempel, P., "Rendezvous zu Einem in Elliptischer Bahn Umlaufenden Ziel," *Astronautica Acta*, Vol. 11, No. 5, 1965, pp. 312–321.

[13] Garrison, J. L., Gardner, T. G., and Axelrad, P., "Relative Motion in Highly Elliptical Orbits," *Advances in the Astronautical Sciences*, Vol. 89, 1995, pp. 1359–1376.

[14] Melton, R. G., "Time-Explicit Representation of Relative Motion Between Elliptical Orbits," *Journal of Guidance, Control, and Dynamics*, Vol. 23, No. 4, July–Aug. 2000, pp. 604–610. doi:10.2514/2.4605

[15] Alfriend, K. T., and Yan, H., "An Evaluation and Comparison of Relative Motion Theories," *Journal of Guidance, Control, and Dynamics*, Vol. 28, No. 2, March–April 2005, pp. 254–263. doi:10.2514/1.6691

[16] Vadali, S. R., Vaddi, S. S., and Alfriend, K. T., "A New Concept for Controlling Formation Flying Satellite Constellations," *Advances in the Astronautical Sciences*, Vol. 108, 2001, pp. 1631–1648.

[17] Paschmann, G., and Daly, P. W., *Analysis Methods for Multi-Spacecraft Data*, ESA Publ., The Netherlands, 1998.

[18] Guzman, J., and Schiff, C., "A Preliminary Study for a Tetrahedron Formation: Quality Factors and Visualization," *AIAA/AAS Astrodynamics Specialist Conference*, Monterey, CA, AIAA Paper 2002-4637Aug. 2002.

[19] Sengupta, P., and Vadali, S. R., "Relative Motion and the Geometry of Formations in Keplerian Elliptic Orbits," *Journal of Guidance, Control, and Dynamics*, Vol. 30, No. 4, July–Aug. 2007, pp. 953–964. doi:10.2514/1.25941

[20] de Pauw, F., Lebeer, C., and Patch, K., "Optimization with Stochastic Parameters in Design of Industrial Air Coolers: the Concept of Shortage Costs," *Engineering Costs and Production Economics*, Vol. 7, No. 2, 1983, pp. 107–118. doi:10.1016/0167-188X(83)90002-2